frontiers | Frontiers in Physics

TYPE Original Research
PUBLISHED 31 July 2023
DOI 10.3389/fphy.2023.1203946

OPEN ACCESS

EDITED BY
Aldo Bonasera,
Texas A&M University, United States

REVIEWED BY
Giuseppe A. Pablo Cirrone,
Laboratori Nazionali del Sud (INFN), Italy
Yan-Fei Li,
Xi'an Jiaotong University, China
Changbo Fu,
Fudan University, China

*CORRESPONDENCE
Baozhen Zhao,
zhaobaozhen@ciae.ac.cn

RECEIVED 11 April 2023
ACCEPTED 20 July 2023
PUBLISHED 31 July 2023

CITATION
Liu Q, Ma M, Zhang X, Lv C, Song J, Wang Z, Yang G, Yang Y, Wang J, Li Q and Zhao B (2023), Characteristic diagnosis of supersonic gas jet target for laser wakefield acceleration with high spatial-temporal resolution Nomarski interference system.
Front. Phys. 11:1203946.
doi: 10.3389/fphy.2023.1203946

Characteristic diagnosis of supersonic gas jet target for laser wakefield acceleration with high spatial-temporal resolution Nomarski interference system

Qiushi Liu[1], Mingjiang Ma[2], Xiaohua Zhang[1], Chong Lv[1], Jianmin Song[3], Zhao Wang[1], Guoqing Yang[1], Yanlei Yang[1], Jiahao Wang[1], Qinxiang Li[1] and Baozhen Zhao[1]*

[1]Department of Nuclear Physics, China Institute of Atomic Energy, Beijing, China, [2]High Intensity Femtosecond Laser Laboratory, Hajim School of Engineering Applied Sciences, Institute of Opitc, University of Rochester, Rochester, NY, United States, [3]Department of MicroSystem Intergration, Beiing Institute of Aerospace Control Devices, Beijing, China

Gas targets hold distinctive significance and advantages in the field of laser-matter interaction. As a major type of gas targets, supersonic gas target is one of the most commonly used targets for laser wakefield acceleration (LWFA). The temporal-spatial resolution study of it could provide valuable data references for the LWFA experiment. In this work, a Nomarski interference system with high spatial-temporal resolution was set up to diagnose the jet process of supersonic gas jet target. The formation process of supersonic gas jet under different jet durations, different injection positions and different gas back pressures was studied. It is beneficial to determine the more optimized time and position of laser injection into target when conducting LWFA experiments. Therefore, the quality of the obtained electron beam and radiation source can be effectively improved.

KEYWORDS

supersonic gas jet, laser wakefield acceleration, optical diagnosis, spatial-temporal resolution, Nomarski interference system

1 Introduction

Gas target plays an important role in laser-matter interaction experiments. It can provide gas with density widely ranging from 10^{16}–10^{21} cm^{-3}, and has the characteristics of adjustable gas density range and controllable gas length [1–6]. Based on the development of chirped-pulse amplification (CPA), the laser acceleration research has made continuous breakthroughs [7–12]. Meanwhile, the research on gas targets has made a lot of progress. The frequently used gas targets in laser acceleration experiments mainly include: gas cell [13–17], capillary [4,18,19], and supersonic gas jet targets [20–25]. The supersonic gas jet target has a De-Laval structure and could produce supersonic gas jet with steep edge and wide flat top area. The gas jet density of such target is relatively uniform and could be controlled by adjusting the back pressure, changing the nozzle structure, and combining multiple nozzles. Its interaction area with laser could cover sub-millimeter to centimeter order, and the nozzle is generally made of stainless steel, which is not easy to be damaged, making it suitable for high repetition rate experiments [26–28] and effectively

reduce the energy spread of accelerated beams [9–11,29,30]. Therefore, it is very suitable as an experimental target for laser wakefield acceleration [25,31,32], laser-driven betatron [33–36] and gamma radiation source [37–40], etc.

To have a deep understanding of the supersonic gas jet targets characteristics, a series of related studies have been carried out [41–45]. The optical interference system could diagnose the density of substance through the interference fringe with advantages including high spatial-temporal resolution, high sensitivity, simple structure, and no influence on the properties of detected substances. It has become a significant diagnostic method in the fields of gas target [46–49], cluster target [50–52], dense plasma [53,54], etc. Commonly used diagnostic systems include Mach-Zehnder interferometer, Michelson interferometer, Nomarsk interferometer and other novel interferometers. Among several interference diagnosis systems, the Nomarski type mainly divides the probe laser into two homologous beam (ordinary light and extraordinary light) through a Wollaston prism, and interference fringes could be obtained in the overlapping area of the two beams. Compared with other systems, the Nomarski type has the characteristics of simple structure, strictly equal optical path, and high stability, which could effectively reduce the size of diagnosis system and stably produce distinct interference fringes. Through various optimizations, the density profile information of supersonic gas jet target can be accurately given. Through various optimizations, the density profile information of supersonic gas jet target can be accurately reconstructed.

For the gas targets used in LWFA, the gas jet density profile generated during laser interaction will ultimately affect the quality of electron beam. The required gas density for LWFA experiments is typically in the range of 10^{17}–10^{19}cm^{-3}, and gas density profile with steep edge and flat top could result in better monoenergetic electron beams. The important parameters affecting the gas density profile mainly include the structural parameters of the target, and the adjustable parameters during experiments, such as gas back pressure, laser injection position, and jet duration.

The duration of the ultra-short pulse laser and gas jet interaction process is usually in the order of few picoseconds. This makes the injection time and position of laser have obvious influence on the accelerating energy and energy dissipation. In order to obtain high quality beams by LWFA, the specific stable duration and exact density distribution of gas jet are needed. To meet the above requirements, the characteristic diagnosis of supersonic gas jet target with high spatial-temporal resolution needs to be systematically carried out.

In this work, a series of studies have been carried out on the spatial-temporal resolution diagnosis of the supersonic gas jet targets. We reported the establishment of a Nomarski interference system with high spatial-temporal resolution and high stability. With the system, the density profile of supersonic gas jet with long injection area could be diagnosed, thus effectively reducing the complexity of the whole experiment. We obtained the multi-frame density profiles of the self-developed gas jet target. In addition, the influences of laser injection position, jet duration and back pressure on the gas jet formation process were studied. Through the experiments, we could determine optimized laser injection time and position into the target, so as to effectively utilize more stable supersonic gas jet with uniform density profile. This work could provide important data and diagnostic method for LWFA experiments to obtain high-quality beams and radiation sources.

2 High spatial-temporal resolution Nomarski interference system

2.1 Experimental setup

The established optical interference system is a modified Nomarski type with vertical fringes, instead of the conventional interference systems with horizontal fringes. Based on our previous studies [55,56], such type of Nomarski interference system has better experimental performance in diagnosis stability and accuracy than normal Mach-Zehnder interferometer. Compared with the conventional Nomarski interferometer, it could guarantee the integrity of gas jet imaged on the interference area. These features make it possible to meet the actual experimental requirements and realize the high spatial-temporal resolution of gas target characteristics through an ordinary CCD instead of more complicated types with high precision temporal gating. The layout of the system is illustrated in Figure 1.

To realize effective resolution capacity, a pulsed Nd:YAG laser (Q-smart 450 from QUANTEL LASER) is used as the probe laser. The diameter of the laser beam is about 6 mm and the output wavelength is 532 nm after frequency doubling from 1064 nm. The maximum output energy is about 220 mJ per pulse and the pulse duration is about 6 ns. It can meet the accurate diagnosis need of the gas jet process from 10^{-4}–10^{-2}s in the experiment. Uncoated wedge mirrors are arranged in the system to attenuate high laser energy, and the attenuation ratio is about 20 times to meet the actual experimental requirements. The probe laser is expanded by Keplerian beam expander to 10 mm diameter, so as to ensure that sufficient interference areas are generated subsequently. A 50 μm pinhole is set at the focus as a spatial filter to improve the beam quality, effectively ensuring the generation of distinct interference fringes in the CCD visual field. The polarization ratio of the laser beam is adjusted by a polarizer, and then the laser passes through the gas jet region in a target chamber with high vacuum. The relative position of laser and the gas jet can be accurately adjusted through a 3-axis stage with high precision. After obtaining the gas jet density information, the probe laser was divided into ordinary light (o-light) and extraordinary light (e-light) by a Wollaston prism with a small separation angle. Interference fringes are generated in the overlapping area of two lights, and finally imaged on the CCD for image data acquisition.

In the diagnosis system, the pixel size of CCD is 3.69 μm × 3.69 μm and the imaging area is 1 mm × 1.2 mm. For the overall design, the requirements to be considered include the effective clear aperture of optical elements such as prisms, the overall size control of the system, and obtaining complete information of the gas jet. The imaging lens F3 with a focal length of 450 mm is selected, the object distance is controlled to be 1200 mm and the image distance is 720 mm. Through the overall optical design, the system achieves a magnification of 0.6 and a spatial resolution of approximately 6 μm, enabling diagnosis of centimeter-scale gas jet density profiles. To achieve accurate temporal resolution, the relative delay of

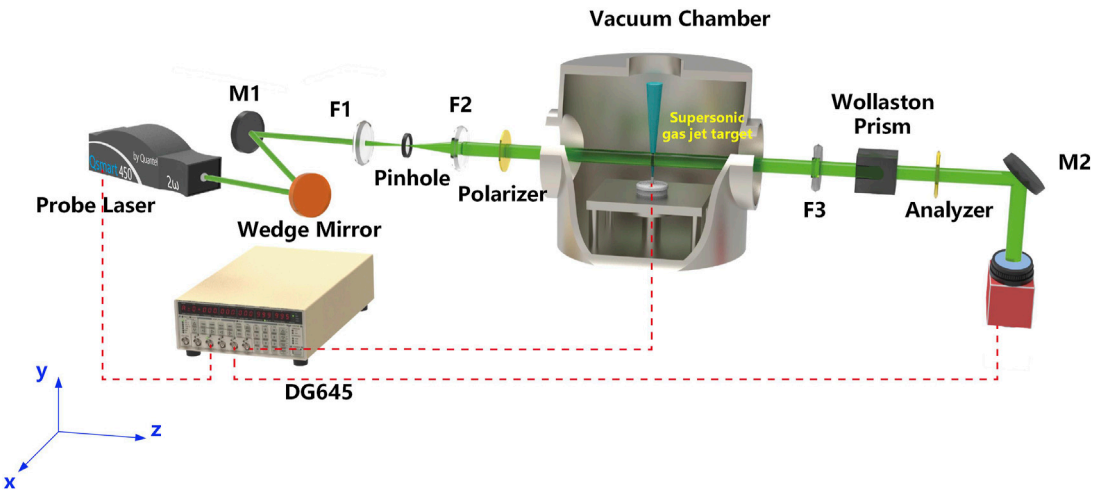

FIGURE 1
Layout of Nomarski interference system with spatial-temporal resolution for gas jet target diagnosis.

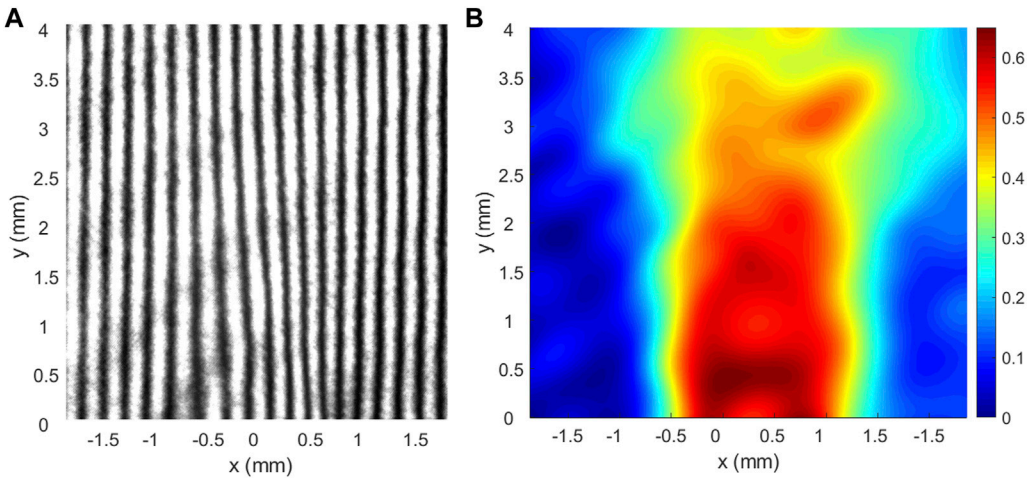

FIGURE 2
The interference fringes and phase difference diagram obtained in the experiment: **(A)** the interference fringes changed during the jet process, **(B)** the phase difference diagram obtained by Abel inversion.

Qsmart-450, gas jet target, and CCD is adjusted by a digital delay generator (Stanford DG645). The pulse duration of the probe laser is about 6 ns. By adjusting the relative delay of the whole system, the temporal resolution can reach about 6 ns, which could meet the accurate diagnosis need of the gas jet process from 10^{-4}–10^{-2}s. The preliminary results show that the self-made gas target could maintain a relatively stable jet ability. In the experiment, the relative delay between laser pulse and gas jet is adjusted. With multiple times experiments, the interference images under different delay conditions could be collected. After Abel inversion processing, the accurate distribution of gas density at different times could be restored, as shown in Figure 2.

Due to the limitations of mechanical processing and the pressure resistance of electromagnetic valves, the throat and outlet dimensions of gas jet targets in LWFA experiments typically range from hundreds of micrometers to several centimeters. To achieve a density of 10^{17}–10^{19} cm^{-3}, the commonly used gas back pressure is generally controlled within several tens of bar. Furthermore, to avoid the vacuum reduction caused by long-duration gas jetting, the jet duration should be kept as short as possible. To prevent damage to the nozzle due to laser jitter, the laser injection needs to be positioned a certain distance. Therefore, according to the above-mentioned related parameters, we carried out the temporal-spatial resolution study on gas back pressure, laser injection position and jet duration.

The nozzle generating a supersonic gas jet in the experiment had De-Laval structure with central symmetry, of which contraction and expansion sections were both conical with a narrow throat in the

middle. The subsonic gas jet was accelerated in the contraction section, then reached the sound speed at the throat with the smallest cross section, and finally entered the expansion section to accelerate to the supersonic speed. A nozzle with 1 mm throat size and 2 mm outlet size was selected for experiments, and the gas was high-purity argon.

2.2 Analytical method

The o-light and e-light generated by the Wollaston prism in the system have the characteristics of strictly equal optical path and direct temporal–spatial coherence. Through parameter design, vertical interference fringes could be produced in the overlapping area. When the probe laser passes through the high-density gas jet area in optical path, the refractive index of this area changes compared with that without gas. Therefore, different refractive indexes form optical path difference manifested by the change of fringes' local width. Here, we set the gas jet flows along y direction, and the laser beam propagates along z direction. The optical path difference could be calculated by integrating the refractive index in the gas jet area:

$$\delta(x,y) = \int \eta_2(x,y,z) - \eta_1(x,y,z)\,dz \tag{1}$$

where η_1 and η_2 are the refractive index of vacuum and gas jet respectively. Converting the optical path difference to phase shift $\Delta\varphi$, we could get:

$$\begin{aligned}\Delta\varphi(x,y) &= \frac{2\pi}{\lambda}\delta(x,y)\\ &= \frac{2\pi}{\lambda}\int_{-\infty}^{\infty}\left[\eta_2(x,y,z) - \eta_1(x,y,z)\right]dz\end{aligned} \tag{2}$$

where λ presents the laser wavelength. The gas target used in this case has a conical De-Laval structure, and the generated gas jet could be considered as central symmetry. The distance that laser travels inside the gas jet could be expressed as:

$$r = \sqrt{x^2 + z^2} \tag{3}$$

Plugging Eq. 3 into Eq. 2, through Abel inversion, we could get the equation calculating refractive index according to phase difference:

$$n(x,y) - 1 = -\frac{\lambda}{2\pi}\int_r^{infty}\frac{\partial\varphi(x,y)}{\partial x}\frac{1}{\sqrt{x^2 - r^2}}\,dx \tag{4}$$

Based on the Lorentz-Lorenz equation [57,58], the gas refractive index is proportional to its particle density and related to the probe laser wavelength. Thus, the gas density profiles could be calculated.

3 Result and discussion

For the supersonic gas jet used in LWFA, the key parameters that affect its gas density distribution and can be adjusted during experiments mainly include gas back pressure, laser injection position and jet duration. In this work, after verifying the temporal-spatial resolution capability of the diagnostic system, we primarily focused on these parameters to investigate their impact on the gas density profile.

We firstly carried out the verification experiments for the spatial-temporal resolution capacity of the system. The jet duration was set to 1 ms and the back pressure was 20 bar. The whole jet formation process could be divided into two stages–the rising stage and the stable stage. Considering the overall experimental requirements, samples were taken every 20 μs within 100 μs from jet progress starting, every 50 μs after 100–500 μs, and every 100 μs after 500 μs. The experimental results were compared with the simulation results, as shown in Figure 3. The simulation in this paper was performed by Computational Fluid Dynamics (CFD). The explicit density-based solver in ANSYS-Fluent was used to simulate the variation of gas jet over time. The comparison showed the experimental data were in good agreement with the simulation data. They both showed after the nozzle opened, the gas density appeared to a gradual upward trend, and the rising duration was about 150–200 μs. Then the density reached a relatively stable stage, maintaining the whole jet progress. The experimental results are generally higher than the simulated values. The reason might be that the actual roughness of nozzle inner surface is higher than the simulation, making the gas jet velocity decrease and the density increase. Through experimental and simulation studies, we have verified the temporal-spatial resolution capability of the established Nomarski interference system. With the electromagnetic valve opening, the valve spring compresses and the piston gradually opens. The gas output increases gradually, and the density will go through a rising stage. Once the piston is fully pulled down, the gas density stabilizes. By controlling the relative delay of laser reaching the target, we could make the laser inject to the gas jet target at the stable section, ensuring the quality of accelerated particles and radiation sources in LWFA experiments.

When injected into the gas target, the laser injection position is one of the adjustable parameters in the experiment, and different injection positions will result in different density values. To ensure that the gas density profile has steep edge and flat top, the distance between laser and nozzle outlet should not be too far. Furthermore, it is necessary to prevent nozzle damage caused by laser jitter when the distance is too close. Therefore, the laser injection is positioned at a distance of a few hundred micrometers to a few millimeters above the nozzle outlet. In the experiment, we selected the density profile at distances of 0.5, 1, 2, and 4 mm from the outlet. In the rising stage of 20 μs, the density was generally low, and the flat-top area was irregular or even not generated, as shown in Figure 4A. At this stage, laser injection would have an adverse effect on the experimental results. When the jet reached the stable stage (as shown in Figure 4B), the flat-top area basically maintained a certain density value. The experimental results match the actual electromagnetic valve opening process of the gas target. During the rising stage, the piston is gradually pulled down, leading to an increasing gas output that prevents the formation of a stable supersonic jet. Once the piston is fully pulled down, the gas target structure conforms to the De-Laval structure required for generating supersonic jet, resulting in a flat-top gas density profile suitable for LWFA experiments. By injecting laser at this stage, the electron beam with better quality could be obtained. Since different positions could produce corresponding density profiles, we could

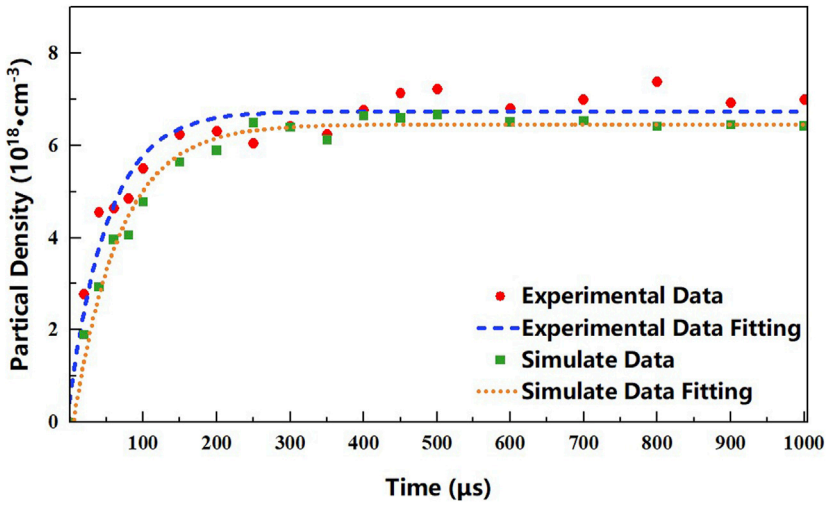

FIGURE 3
Comparison of gas jet formation process between experimental data and simulation (jet duration: 1 ms, back pressure: 20 bar).

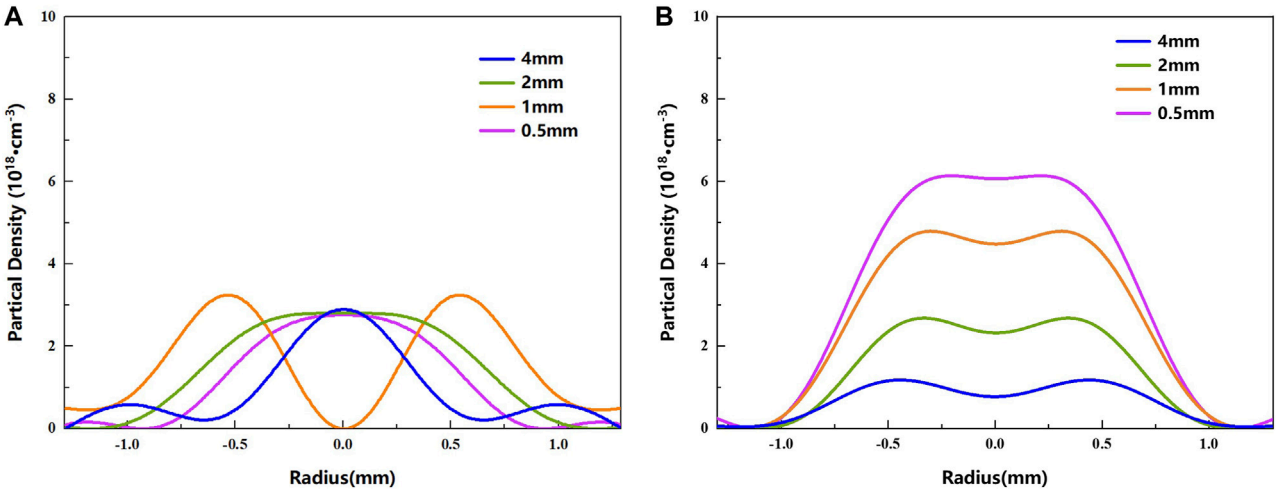

FIGURE 4
The gas jet density profile at multiple laser injection positions in different stages: **(A)** t = 20 ms (rising stage), **(B)** t = 150 ms (stable stage).

adjust the relative position between laser and target according to the actual experimental requirements.

Jet duration is also an important adjustable parameter in LWFA experiments. The electromagnetic valve control device of the gas target typically allows jet durations ranging from microseconds to tens of seconds. Due to the requirement of high vacuum conditions (below 10^{-4} bar) and the need to avoid damage to optical components while obtaining high-quality electron beams, it is necessary to minimize the jet duration in LWFA experiments, especially in high repetition rate experiments. As previous works did not extensively investigate the influence of different jet durations on the gas jet formation process, we conducted experiments under various selected jet durations (0.5 ms, 1 ms, 10 ms and 50 ms respectively). We recorded multi-frame interference images and acquired variation of gas jet density under jet duration after calculation and processing. The comparison of density changes at 0.5 mm above the nozzle is shown in Figure 5. It could be analyzed that the time required to reach the stable stage is basically the same under four typical duration, which is about 150 μs–200 μs. In all four cases, a certain density value could be maintained after being stable. Experimental results show that, under the same back pressure and injection position, the formation of the gas jet exhibits consistent time for rising stage, with little influence from the jet duration. For the same kind of gas target, when the back pressure is constant, the time for the spring and piston to

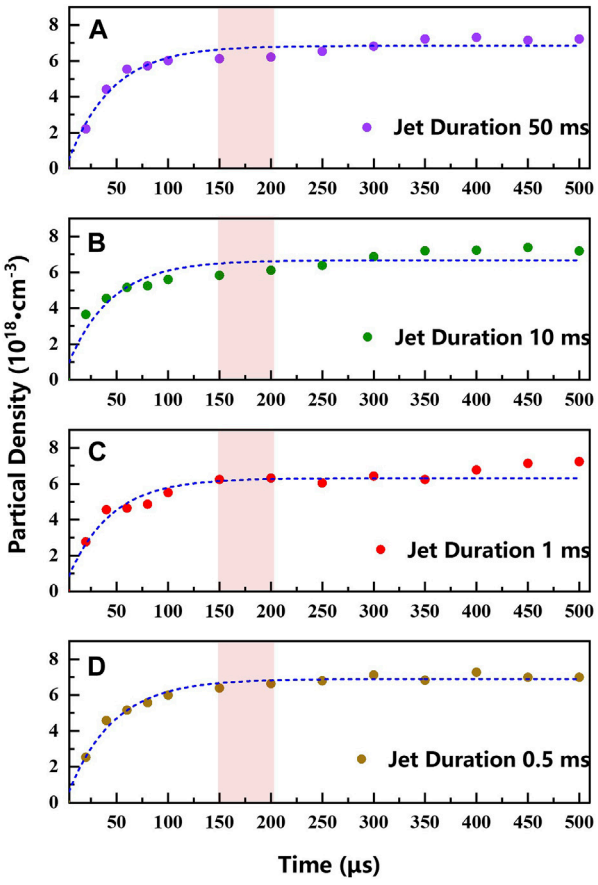

FIGURE 5
Variation of gas jet density under typical jet duration (back pressure 20bar): **(A)** 50 ms, **(B)** 10 ms, **(C)** 1 ms, **(D)** 0.5 ms.

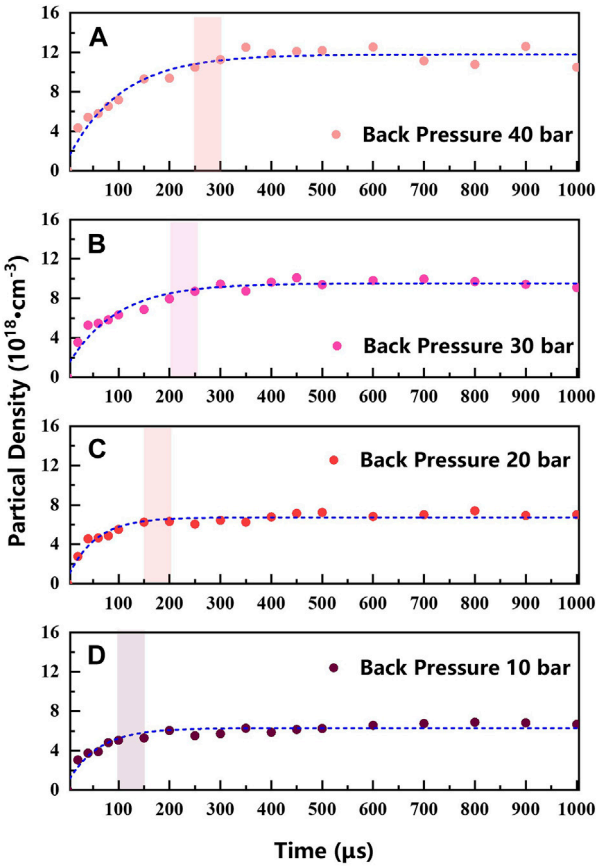

FIGURE 6
Variation of gas jet density under typical back pressure (jet duration 1 ms): **(A)** 40bar, **(B)** 30bar, **(C)** 20bar and **(D)** 10bar.

completely pulled down during the valve opening process is consistent. After fully pulling apart, the jet will enter the stable stage, maintaining the De-Laval structure and continuously provide a stable supersonic gas jet.

The value of gas back pressure could directly affect the gas jet density. The required gas density in LWFA is generally in the range of 10^{17}–10^{19} cm^{-3}. To generate such high-density jets with small-sized and finely structured De-Laval supersonic nozzles, the back pressure is often set to several tens of bar. Therefore, we conducted experiments to compare the effects of various typical back pressures on the gas jet formation process. With 1 ms jet duration, the gas density changes under typical back pressure (10, 20, 30 and 40 bar) were measured, as shown in Figure 6. Under four conditions, the formation process of gas jet accords with rising stage and stable stage. However, when the back pressure increases, the duration of rising stage will gradually increase. With the back pressure increasing from 10 bar to 40 bar, the rising duration increases, ranging from about 100 μs to 300 μs. Increasing the gas back pressure in the experiment results in an extended duration for rising stage. This is because when opening the valve, the increased back pressure increases the pressure acting on the piston, prolonging the time for the spring to fully pull down the piston and delaying the achievement of the stable supersonic jet. Accordingly, when the back pressure changes, in order to ensure the interaction time between laser and gas jet in the stable stage, it is essential to adjust the delay of laser reaching the target according to the actual situation.

4 Conclusion

In this paper, we set up a Nomarski interference system with high stability and spatial-temporal resolution, suitable for the multi-frame diagnosis of supersonic gas jet in LWFA experiment. The temporal resolution reached 6ns and the spatial resolution reached 6 μm. Because of the high stability and vertical interference fringe distribution, the system could realize the temporal resolution without using high-precision ICCD. Thus, the complexity of the system was effectively simplified, and the gas density with a large jet range was ensured to be accurately obtained. The experimental measurement results were in good agreement with the simulations, verifying the performance of the diagnosis system. With data processing, the densities at specific time points in the whole jet process were measured, and the density profile at different time points at multiple laser injection positions could be given. Furthermore, the factors related to the generation process of gas jet, such as back pressure and jet

duration, were systematically studied, and the data under typical back pressure and jet duration conditions were obtained. This work could provide significant experimental methods and data support for LWFA, expecting to improve the quality of the obtained electron beam and radiation source.

Data availability statement

The raw data supporting the conclusion of this article will be made available by the authors, without undue reservation.

Author contributions

QSL, MM, XZ, CL, JS, ZW, GY, YY, JW, QXL, and BZ contributed to the study conception and design. QSL, MM, BZ, and XZ carried out experiments. QSL, CL, JS, GY, and JW performed data analysis. QSL, ZW, YY, and BZ set up the optical diagnosis system. The first draft of the manuscript was written by QSL and MM. All authors contributed to the article and approved the submitted version.

Funding

This work was supported by the Programs for the National Natural Science Foundation of China (Nos 12105371 and 12005305) and the Continuous Basic Scientific Research Project (Nos WDJC-2019-02, BJ20002501 and BJ22003001).

Conflict of interest

The authors declare that the research was conducted in the absence of any commercial or financial relationships that could be construed as a potential conflict of interest.

Publisher's note

All claims expressed in this article are solely those of the authors and do not necessarily represent those of their affiliated organizations, or those of the publisher, the editors and the reviewers. Any product that may be evaluated in this article, or claim that may be made by its manufacturer, is not guaranteed or endorsed by the publisher.

References

1. Nakajima K, Fisher D, Kawakubo T, Nakanishi H, Ogata A, Kato Y, et al. Observation of ultrahigh gradient electron acceleration by a self-modulated intense short laser pulse. *Phys Rev Lett* (1995) 74:984. doi:10.1103/physrevlett.75.984.2

2. Modena A, Najmudin Z, Dangor A, Clayton C, Marsh K, Joshi C, et al. Electron acceleration from the breaking of relativistic plasma waves. *nature* (1995) 377:606–8. doi:10.1038/377606a0

3. Malka V, Faure J, Marques J, Amiranoff F, Rousseau J-P, Ranc S, et al. Characterization of electron beams produced by ultrashort (30 fs) laser pulses. *Phys Plasmas* (2001) 8:2605–8. doi:10.1063/1.1374584

4. Gonsalves A, Nakamura K, Daniels J, Benedetti C, Pieronek C, De Raadt T, et al. Petawatt laser guiding and electron beam acceleration to 8 GeV in a laser-heated capillary discharge waveguide. *Phys Rev Lett* (2019) 122:084801. doi:10.1103/physrevlett.122.084801

5. Fedorets P, Zheng C, Engels R, Engin I, Feilbach H, Giesen U, et al. A high-density polarized ^{3}He gas–jet target for laser–plasma applications. *Instruments* (2022) 6:18. doi:10.3390/instruments6020018

6. Wang W, Feng K, Ke L, Yu C, Xu Y, Qi R, et al. Free-electron lasing at 27 nanometres based on a laser wakefield accelerator. *Nature* (2021) 595:516–20. doi:10.1038/s41586-021-03678-x

7. Krushelnick K, Clark E, Najmudin Z, Salvati M, Santala M, Tatarakis M, et al. Multi-MeV ion production from high-intensity laser interactions with underdense plasmas. *Phys Rev Lett* (1999) 83:737–40. doi:10.1103/physrevlett.83.737

8. Malka V, Fritzler S, Lefebvre E, Aleonard M-M, Burgy F, Chambaret J-P, et al. Electron acceleration by a wake field forced by an intense ultrashort laser pulse. *Science* (2002) 298:1596–600. doi:10.1126/science.1076782

9. Faure J, Glinec Y, Pukhov A, Kiselev S, Gordienko S, Lefebvre E, et al. A laser–plasma accelerator producing monoenergetic electron beams. *Nature* (2004) 431:541–4. doi:10.1038/nature02963

10. Geddes C, Toth C, Van Tilborg J, Esarey E, Schroeder C, Bruhwiler D, et al. High-quality electron beams from a laser wakefield accelerator using plasma-channel guiding. *Nature* (2004) 431:538–41. doi:10.1038/nature02900

11. Mangles SP, Murphy C, Najmudin Z, Thomas AGR, Collier J, Dangor AE, et al. Monoenergetic beams of relativistic electrons from intense laser–plasma interactions. *Nature* (2004) 431:535–8. doi:10.1038/nature02939

12. Willingale L, Mangles S, Nilson P, Clarke R, Dangor A, Kaluza M, et al. Collimated multi-MeV ion beams from high-intensity laser interactions with underdense plasma. *Phys Rev Lett* (2006) 96:245002. doi:10.1103/physrevlett.96.245002

13. Osterhoff J, Popp A, Major Z, Marx B, Rowlands-Rees T, Fuchs M, et al. Generation of stable, low-divergence electron beams by laser-wakefield acceleration in a steady-state-flow gas cell. *Phys Rev Lett* (2008) 101:085002. doi:10.1103/physrevlett.101.085002

14. Brandi F, Giammanco F, Conti F, Sylla F, Lambert G, Gizzi L. Note: Real-time monitoring via second-harmonic interferometry of a flow gas cell for laser wakefield acceleration. *Rev Scientific Instr* (2016) 87:086103. doi:10.1063/1.4960399

15. Liu J, Xia C, Wang W, Lu H, Wang C, Deng A, et al. All-optical cascaded laser wakefield accelerator using ionization-induced injection. *Phys Rev Lett* (2011) 107:035001. doi:10.1103/physrevlett.107.035001

16. Wang X, Zgadzaj R, Fazel N, Li Z, Yi S, Zhang X, et al. Quasi-monoenergetic laser-plasma acceleration of electrons to 2 GeV. *Nat Commun* (2013) 4:1988. doi:10.1038/ncomms2988

17. Aniculaesei C, Kim HT, Yoo BJ, Oh KH, Nam CH. Novel gas target for laser wakefield accelerators. *Rev Scientific Instr* (2018) 89:025110. doi:10.1063/1.4993269

18. Leemans WP, Nagler B, Gonsalves AJ, Tóth C, Nakamura K, Geddes CG, et al. GeV electron beams from a centimetre-scale accelerator. *Nat Phys* (2006) 2:696–9. doi:10.1038/nphys418

19. Leemans W, Gonsalves A, Mao H-S, Nakamura K, Benedetti C, Schroeder C, et al. Multi-GeV electron beams from capillary-discharge-guided subpetawatt laser pulses in the self-trapping regime. *Phys Rev Lett* (2014) 113:245002. doi:10.1103/physrevlett.113.245002

20. Semushin S, Malka V. High density gas jet nozzle design for laser target production. *Rev Scientific Instr* (2001) 72:2961–5. doi:10.1063/1.1380393

21. Krishnan M, Wright J, Ma T. A fast, electromagnetically driven supersonic gas jet target for laser wakefield acceleration. *AIP Conf Proc* (2009) 1086:264–9. doi:10.1063/1.3080916

22. Schmid K, Veisz L. Supersonic gas jets for laser-plasma experiments. *Rev Scientific Instr* (2012) 83:053304. doi:10.1063/1.4719915

23. Burza M, Gonoskov A, Svensson K, Wojda F, Persson A, Hansson M, et al. Laser wakefield acceleration using wire produced double density ramps. *Phys Rev Spec Topics-Accelerators Beams* (2013) 16:011301. doi:10.1103/physrevstab.16.011301

24. Sylla F, Veltcheva M, Kahaly S, Flacco A, Malka V. Development and characterization of very dense submillimetric gas jets for laser-plasma interaction. *Rev Scientific Instr* (2012) 83:033507. doi:10.1063/1.3697859

25. Wang W, Li W, Liu J, Zhang Z, Qi R, Yu C, et al. High-brightness high-energy electron beams from a laser wakefield accelerator via energy chirp control. *Phys Rev Lett* (2016) 117:124801. doi:10.1103/physrevlett.117.124801

26. Salehi F, Goers A, Hine G, Feder L, Kuk D, Miao B, et al. MeV electron acceleration at 1 kHz with <10 mJ laser pulses. *Opt Lett* (2017) 42:215–8. doi:10.1364/ol.42.000215

27. Guénot D, Gustas D, Vernier A, Beaurepaire B, Böhle F, Bocoum M, et al. Relativistic electron beams driven by kHz single-cycle light pulses. *Nat Photon* (2017) 11:293–6. doi:10.1038/nphoton.2017.46

28. Salehi F. *High repetition rate laser-driven electron acceleration to mega-electron-volt energies*. College Park: University of Maryland (2019). Ph.D. thesis.

29. Zeng M, Chen M, Yu L-L, Mori WB, Sheng Z-M, Hidding B, et al. Multichromatic narrow-energy-spread electron bunches from laser-wakefield acceleration with dual-color lasers. *Phys Rev Lett* (2015) 114:084801. doi:10.1103/physrevlett.114.084801

30. Wang W, Li W, Liu J, Wang C, Chen Q, Zhang Z, et al. Control of seeding phase for a cascaded laser wakefield accelerator with gradient injection. *Appl Phys Lett* (2013) 103:243501. doi:10.1063/1.4842236

31. Sylla F, Flacco A, Kahaly S, Veltcheva M, Lifschitz A, Malka V, et al. Short intense laser pulse collapse in near-critical plasma. *Phys Rev Lett* (2013) 110:085001. doi:10.1103/physrevlett.110.085001

32. Lemos N, Lopes N, Dias J, Viola F. Design and characterization of supersonic nozzles for wide focus laser-plasma interactions. *Rev Scientific Instr* (2009) 80:103301. doi:10.1063/1.3233895

33. Rousse A, Phuoc KT, Shah R, Pukhov A, Lefebvre E, Malka V, et al. Production of a kev x-ray beam from synchrotron radiation in relativistic laser-plasma interaction. *Phys Rev Lett* (2004) 93:135005. doi:10.1103/physrevlett.93.135005

34. Corde S, Phuoc KT, Lambert G, Fitour R, Malka V, Rousse A, et al. Femtosecond x rays from laser-plasma accelerators. *Rev Mod Phys* (2013) 85:1–48. doi:10.1103/revmodphys.85.1

35. Phuoc KT, Corde S, Shah R, Albert F, Fitour R, Rousseau J-P, et al. Imaging electron trajectories in a laser-wakefield cavity using betatron x-ray radiation. *Phys Rev Lett* (2006) 97:225002. doi:10.1103/physrevlett.97.225002

36. Lu Y, Zhang G-B, Zhao J, Hu Y-T, Zhang H, Li D-A, et al. Ultra-brilliant GeV betatronlike radiation from energetic electrons oscillating in frequency-downshifted laser pulses. *Opt Express* (2021) 29:8926–40. doi:10.1364/oe.419761

37. Irani E, Omidvar H, Sadighi-Bonabi R. Gamma rays transmutation of palladium by bremsstrahlung and laser inverse Compton scattering. *Energ Convers Manag* (2014) 77:558–63. doi:10.1016/j.enconman.2013.09.029

38. Li D, Imasaki K, Horikawa K, Miyamoto S, Amano S, Mochizuki T. Iodine transmutation through laser Compton scattering gamma rays. *J Nucl Sci Technol* (2009) 46:831–5. doi:10.1080/18811248.2007.9711592

39. Xu H-H, Wu H-L, Fan G-T, Chen J-H, Wang D. A new consecutive energy calibration method for x/γ detectors based on energy continuously tunable laser Compton scattering light source. *Nucl Sci Tech* (2017) 28:121. doi:10.1007/s41365-017-0272-1

40. Zhu X-L, Chen M, Weng S-M, Yu T-P, Wang W-M, He F, et al. Extremely brilliant GeV γ-rays from a two-stage laser-plasma accelerator. *Sci Adv* (2020) 6:eaaz7240. doi:10.1126/sciadv.aaz7240

41. Malka V, Coulaud C, Geindre J, Lopez V, Najmudin Z, Neely D, et al. Characterization of neutral density profile in a wide range of pressure of cylindrical pulsed gas jets. *Rev Scientific Instr* (2000) 71:2329–33. doi:10.1063/1.1150619

42. Landgraf B, Schnell M, Sävert A, Kaluza MC, Spielmann C. High resolution 3D gas-jet characterization. *Rev Scientific Instr* (2011) 82:083106. doi:10.1063/1.3624694

43. Lorenz S, Grittani G, Chacon-Golcher E, Lazzarini C, Limpouch J, Nawaz F, et al. Characterization of supersonic and subsonic gas targets for laser wakefield electron acceleration experiments. *Matter Radiat Extremes* (2019) 4:015401. doi:10.1063/1.5081509

44. Steinke S, Van Tilborg J, Benedetti C, Geddes C, Schroeder C, Daniels J, et al. Multistage coupling of independent laser-plasma accelerators. *Nature* (2016) 530:190–3. doi:10.1038/nature16525

45. Guillaume E, Döpp A, Thaury C, Phuoc KT, Lifschitz A, Grittani G, et al. Electron rephasing in a laser-wakefield accelerator. *Phys Rev Lett* (2015) 115:155002. doi:10.1103/physrevlett.115.155002

46. Hansen A, Haberberger D, Katz J, Mastrosimone D, Follett R, Froula D. Supersonic gas-jet characterization with interferometry and Thomson scattering on the OMEGA Laser System. *Rev Scientific Instr* (2018) 89:10C103. doi:10.1063/1.5036645

47. Nejdl J, Vančura J, Boháček K, Albrecht M, Chaulagain U. Imaging michelson interferometer for a low-density gas jet characterization. *Rev Scientific Instr* (2019) 90:065107. doi:10.1063/1.5098084

48. Feister S, Nees J, Morrison J, Frische K, Orban C, Chowdhury E, et al. A novel femtosecond-gated, high-resolution, frequency-shifted shearing interferometry technique for probing pre-plasma expansion in ultra-intense laser experiments. *Rev Scientific Instr* (2014) 85:11D602. doi:10.1063/1.4886955

49. Chaulagain U, Karatodorov S, RaclavskỲ M, Lorenz S, Lamač M, Albrecht M, et al. Tomographic characterization of gas jets for laser-plasma acceleration with increased sensitivity. Int Conf X-Ray Lasers 2020 *(Spie)* (2021) 11886:61–7. doi:10.1117/12.2592861

50. Jinno S, Kanasaki M, Uno M, Matsui R, Uesaka M, Kishimoto Y, et al. Micron-size hydrogen cluster target for laser-driven proton acceleration. *Plasma Phys Controlled Fusion* (2018) 60:044021. doi:10.1088/1361-6587/aaafa8

51. Goers A, Yoon S, Elle J, Hine G, Milchberg H. Laser wakefield acceleration of electrons with ionization injection in a pure N^{5+} plasma waveguide. *Appl Phys Lett* (2014) 104:214105. doi:10.1063/1.4880102

52. Gao X, Wang X, Shim B, Downer M. Laser-driven acceleration in clustered plasmas. *AIP Conf Proc* (2009) 1086:142–6. doi:10.1063/1.3080895

53. Plateau G, Matlis N, Geddes C, Gonsalves A, Shiraishi S, Lin C, et al. Wavefront-sensor-based electron density measurements for laser-plasma accelerators. *Rev Scientific Instr* (2010) 81:033108. doi:10.1063/1.3360889

54. Zuffi AVF, dos Santos JR, Maldonado EP, Vieira ND, Samad RE. Femtosecond laser-plasma dynamics study by a time-resolved mach–zehnder-like interferometer. *Appl Opt* (2023) 62:C128–C134. doi:10.1364/ao.477395

55. Liu Q, Ma M, Zhang X, Zhao B, Lv C, Meng X, et al. Application of nomarski interference system in supersonic gas-jet target diagnosis. *AIP Adv* (2021) 11:015145. doi:10.1063/5.0027317

56. Liu Q-S, Ma M-J, Zhao B-Z, Zhang X-H, Lv C, Meng X-H, et al. Effect of multiple parameters on the supersonic gas-jet target characteristics for laser wakefield acceleration. *Nucl Sci Tech* (2021) 32:75. doi:10.1007/s41365-021-00910-1

57. Lorentz HA. Ueber die beziehung zwischen der fortpflanzungsgeschwindigkeit des lichtes und der körperdichte. *Annalen der Physik* (1880) 245:641–65. doi:10.1002/andp.18802450406

58. Lorenz L. Ueber die refractionsconstante. *Annalen der Physik* (1880) 247:70–103. doi:10.1002/andp.18802470905